BMC Veterinary Research

RESEARCH

Open Access

Magnetic resonance imaging of the dromedary camel carpus

Ayman El Nahas[1] and Usama Hagag[1,2*]

Abstract

Background The dromedary camel (Camelus dromedarius) carpal joint presents multiple joints and constitutes several bones and soft tissues. Radiography and/or ultrasonography of the carpus are challenging due to structural superimposition. High-field magnetic resonance imaging (MRI) technique precludes superimposed tissues and offers high soft tissue contrast in multiple sequences and planes. Hence, understanding the normal MRI anatomy is crucial during clinical investigations. Magnetic resonance imaging is highly sensitive for investigation of soft tissues and articular cartilage; therefore, it is extensively used for outlining joint anatomy and evaluation of a wide range of musculoskeletal conditions. MRI images of a specific anatomical region acquired by using multiple sequences in various planes are necessary for a complete MRI examination. Given the dearth of information on the MRI features of the dromedary camel carpus, the current study demonstrates the MRI appearance of the clinically significant structures in the camel carpus in various sequences and planes using a high-field 1.5 Tesla superconducting magnet. For this purpose, twelve cadaveric forelimbs, obtained from 6 clinically sound lameness free adult dromedary camels, were examined.

Results The cortex and medulla of the radius, carpal bones and metacarpus were evaluated. Articular cartilage of the carpal joints was depicted and showed intermediate intensity. Carpal tendons expressed lower signal intensity in all pulse sequences. The collateral and inter-carpal ligaments showed mixed signal intensity.

Conclusions The obtained data outlines the validation of MRI for investigation of the camel carpus and could set as a reference for interpretation in clinical patients.

Keywords MRI, Camel, Carpus, Imaging

Background

The dromedary camel carpus is a complex joint between the antebrachium and the proximal metacarpus and involves multiple bones and ligaments and surrounded by numerous tendons. The carpal bones of camel are arranged in two rows. The upper row comprises the radial, intermediate, ulnar, and accessory carpal bones, and the lower row contains the second, third, and fourth carpal bones. The carpal articulations comprise the antebrachiocarpal, midcarpal, and the carpometacarpal joints. Carpal bones arrangement is supported by the surrounding soft tissues represented by the fibrous joint

*Correspondence:
Usama Hagag
usama.hagag@vet.bsu.edu.eg; uhagag@kfu.edu.sa
[1]Department of Clinical Sciences, College of Veterinary Medicine, King Faisal University, PO Box 400, Al-Ahasa 31982, Saudi Arabia
[2]Department of Surgery, Anesthesiology and Radiology, Faculty of Veterinary Medicine, Beni-Suef University, Beni-Suef 62511, Egypt

capsule and the collateral, inter-carpal and palmar ligaments [1].

The carpus is a frequently injured joint in camels and pain originating from the carpus is a pervasive difficulty, particularly in athletic camels [2, 3]. Carpal pain and joint effusion can be easily recognized dorsally on the joint [4]; however, the multifaceted structure of the carpus restricts physical examination and limits the ability of radiography and/or ultrasonography to assess carpal injury [5]. MRI has great potential in the assessment of various bony and soft tissue structures and has been clinically beneficial for investigation of musculoskeletal disorders including the carpus [6–8]. MRI exhibits numerous advantages for diagnosing musculoskeletal disorders as it enables accurate visualization of subchondral bone, articular cartilage, synovial fluid, ligaments and tendons [9–12].

Owing to the complex anatomy, numerous pathologies, and the presence of a myriad of injury mechanisms in the carpal region, MRI protocols and sequences should ensure detailed and accurate assessment of both bones and soft tissues [13]. Therefore, understanding carpal anatomy and the difference between the normal and injured MRI appearance of the clinically relevant structures are crucial for decisive diagnosis. Previous studies on the camel carpus included a general anatomic description [14], radiographic and ultrasonographic investigations [2] and computed tomography [3]. To date, there is limited information on using MRI in the camel carpus. Therefore, our objectives were to develop a high-field MRI procedure for exploration of camel carpus and to report the normal signal intensity of various carpal structures on the obtained high-field MRI images.

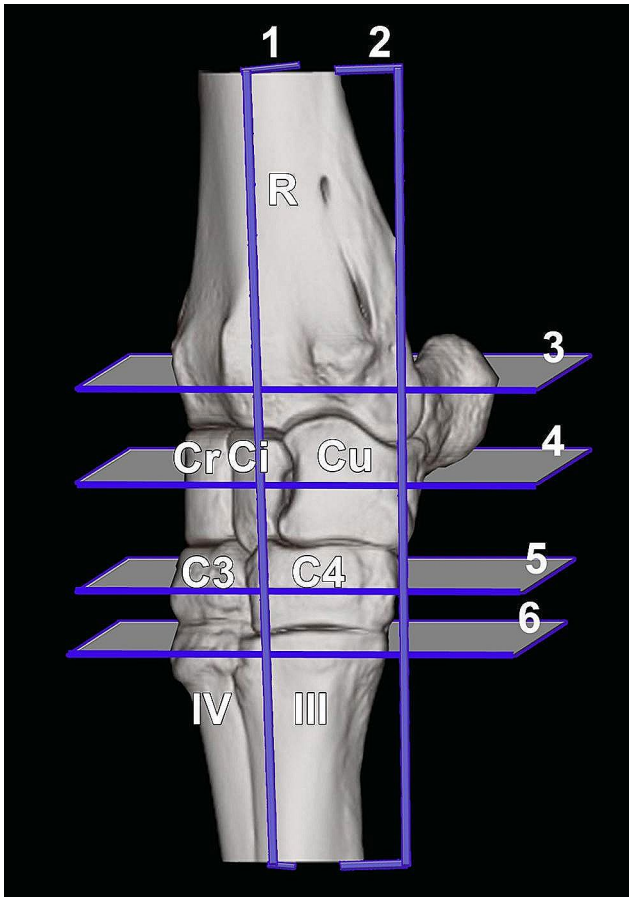

Fig. 1 Three-dimensional reconstructed dorsolateral view of the normal dromedary camel carpus. Numbered sections (sagittal, 1; dorsal, 2; and transverse, 3–6) indicate the approximate levels of the selected magnetic resonance images. R, radius; Cu, ulnar carpal bone; Ci, intermediate carpal bone; Cr, radial carpal bone; C3, 3rd carpal bone; C4, fourth carpal bone; III, 3rd metacarpal bone; VI, fourth metacarpal bone

Results

All osseous components of the dromedary carpus were seen on all MRI pulse sequences and were illustrated in the three-dimensional reconstructed dorsolateral view of the normal dromedary camel carpus. In Fig. 1. numbered sections (sagittal, 1; dorsal, 2; and transverse, 3–6) indicate the approximate levels of the selected magnetic resonance scans. Figure 2, sagittal T1, T2, STIR and PD –weighted MRI sequences obtained in the axial aspect of the carpus at the level of the intermediate carpal bone; Fig. 3, dorsal T1 and T2-weighted MRI sequences at the level of the collateral ligaments; Fig. 4, transverse T1 and T2-weighted MRI sequences at the level of the distal radius; Fig. 5, transverse T1 and T2-weighted and STIR MRI sequences at the level of the proximal row of carpal bones; Fig. 6, transverse T1-weighted and STIR MRI sequences at the level of the distal row of carpal bones; and Fig. 7, transverse T1 and PD-weighted MRI sequences at the level of the proximal metacarpal region). The cortex and subchondral bone had smooth outlines. The radial medulla expressed marked hyperintensity and the cortex showed homogenous hypointensity. The antebrachiocarpal, midcarpal and carpometacarpal articular cartilage was depicted with intermediate signal intensity on the T1- and T2- weighted imaging sequences particularly on the sagittal (Fig. 2) and dorsal (Fig. 3) plane MRI images. The medulla of carpal bones showed decreased intensity compared to the radius and metacarpus in the T1 and T2 images.

The carpus of the dromedary comprised numerous soft tissue structures including the radial carpal extensor, common digital extensor, ulnar carpal extensor, lateral digital extensor, oblique carpal extensor, radial carpal flexor, ulnar carpal flexor, superficial digital flexor (SDFT) and deep digital flexor (DDFT) tendons; the superficial long and deep short divisions of the medial and lateral collateral ligaments; the short inter-carpal and palmar ligaments, and the accessory carpal ligaments.

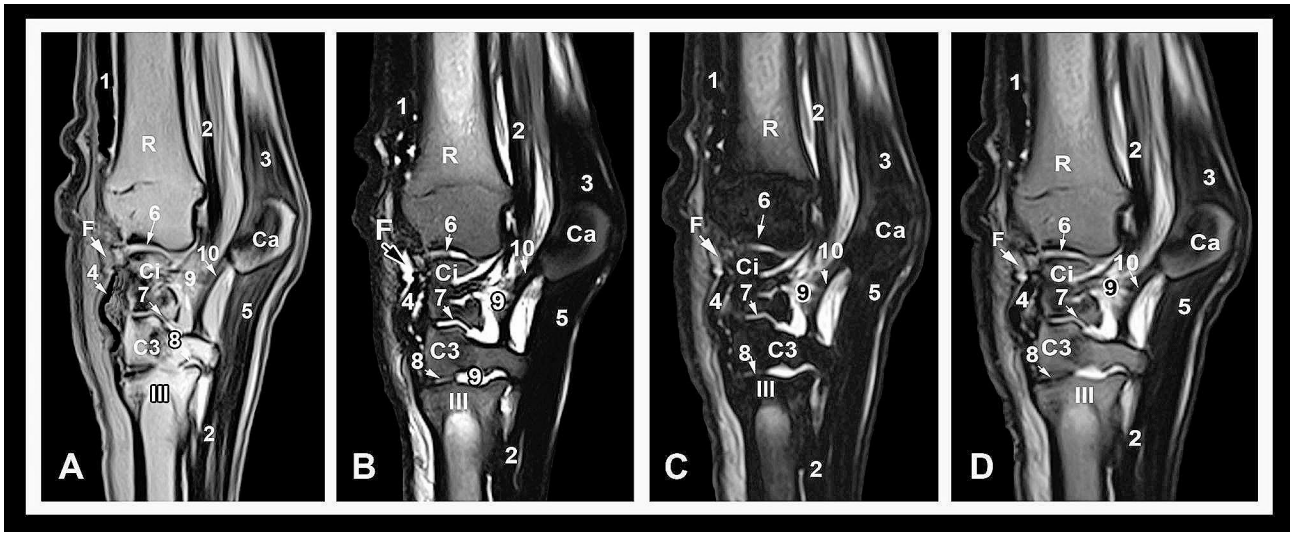

Fig. 2 Sagittal T1 (**A**), T2 (**B**), STIR (**C**) and PD -weighted (**D**) high-filed MRI images obtained in the axial aspect of the carpus at the level of the intermediate carpal bone. Dorsal is to the left. R, radius; Ci, intermediate carpal bone; Ca, accessory carpal bone; III, 3rd metacarpal bone; F, fat pad; 1, common digital extensor tendon; 2, deep digital flexor tendon; 3, ulnar carpal flexor tendon; 4, radial carpal extensor tendon; 5, superficial digital flexor tendon; 6, articular cartilage of the antebrachiocarpal joint; 7, articular cartilage of the middle inter-carpal joint; 8, articular cartilage of the carpo-metacarpal joint; 9, synovial fluid; 10, accessory quartal ligament

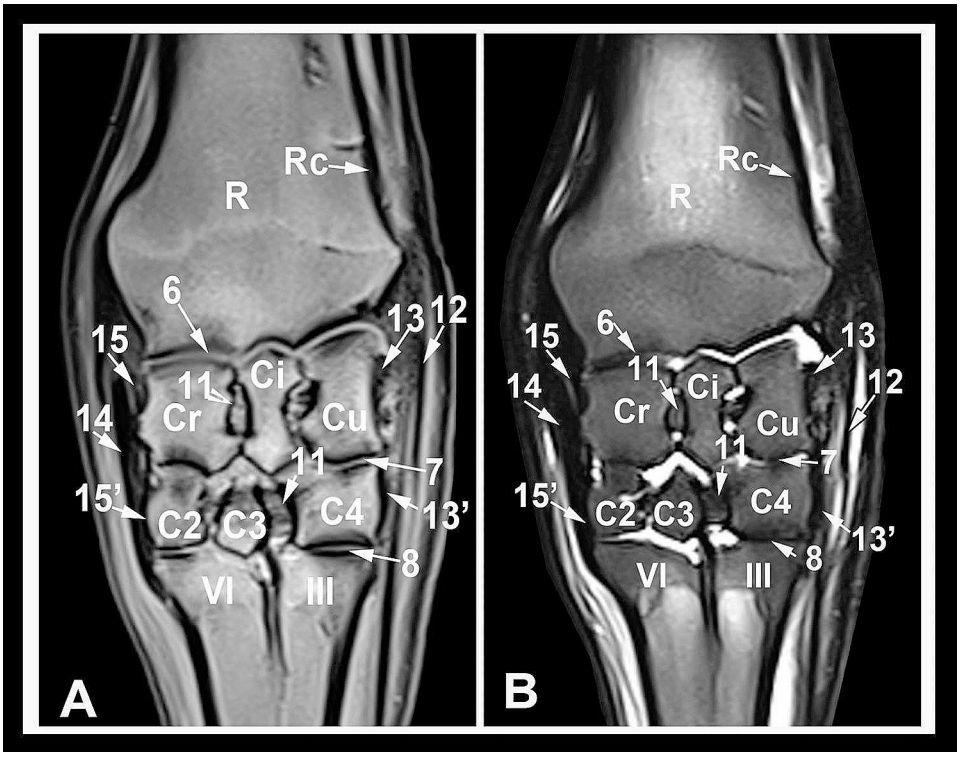

Fig. 3 Dorsal T1 (**A**) and T2-weighted (**B**) high-filed MRI images at the level of the collateral ligaments. R, radius; Rc, radial cortical bone; Cu, ulnar carpal bone; Ci, intermediate carpal bone; Cr, radial carpal bone; C2, 2nd carpal bone; C3, 3rd carpal bone; C4, fourth carpal bone; III, 3rd metacarpal bone; VI, fourth metacarpal bone; 6, articular cartilage of the antebrachiocarpal joint; 7, articular cartilage of the middle inter-carpal joint; 8, articular cartilage of the carpometacarpal joint; 11, short intercarpal ligaments; 12, long lateral collateral carpal ligament; 13, proximal part of the short lateral collateral carpal ligament; 13′, distal part of the short lateral collateral carpal ligament; 14, long medial collateral carpal ligament; 15, proximal part of the short medial collateral carpal ligament; 15′, distal part of the short medial collateral carpal ligament

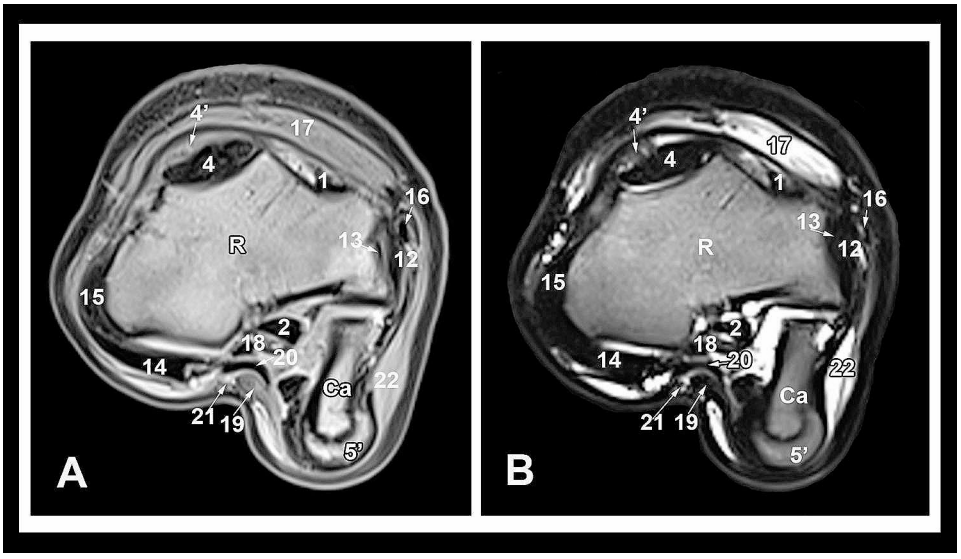

Fig. 4 Transverse T1 (**A**) and T2-weighted (**B**) high-filed MRI images at the level of the distal radius. Medial is to the left. R, radius; Ca, accessory carpal bone; 1, common digital extensor tendon; 2, deep digital flexor tendon; 4, radial carpal extensor tendon; 4', tendon sheath of the radial carpal extensor tendon; 5', origin of the superficial digital flexor tendon; 12, long lateral collateral carpal ligament; 13, proximal part of the short lateral collateral carpal ligament; 14, long medial collateral carpal ligament; 15, proximal part of the short medial collateral carpal ligament; 16, lateral digital extensor tendon; 17, extensor retinaculum; 18, radial carpal flexor tendon; 19, median artery; 20, median vein; 21, median nerve; 22, flexor retinaculum

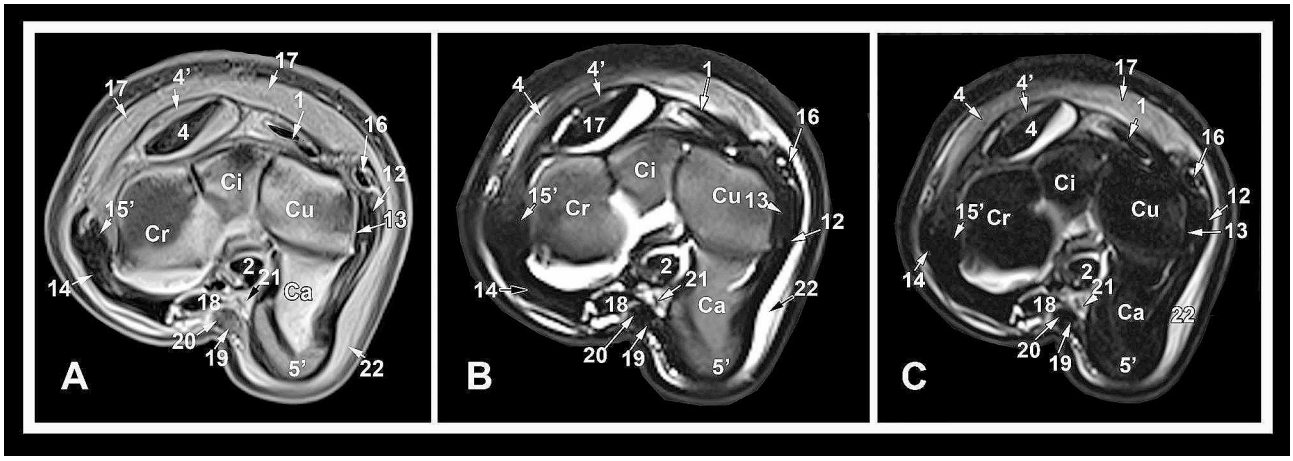

Fig. 5 Transverse T1 (**A**) and T2-weighted (**B**) and STIR (**C**) high-filed MRI images at the level of the proximal row of carpal bones. Cu, ulnar carpal bone; Ci, intermediate carpal bone; Cr, radial carpal bone; Ca, accessory carpal bone; 1, common digital extensor tendon; **2**, deep digital flexor tendon; 4, radial carpal extensor tendon; 4', radial carpal extensor tendon sheath; 5', origin of the superficial digital flexor tendon; 12, long lateral collateral carpal ligament; 13, proximal part of the short lateral collateral carpal ligament; 14, long medial collateral carpal ligament; 15', short medial collateral carpal ligament; 16, lateral digital extensor tendon; 17, extensor retinaculum; 18, radial carpal flexor tendon; 19, median artery; 20, median vein; 21, median nerve; 22, flexor retinaculum

The radial carpal extensor tendon was observed while crossing the dorsal surface of the carpal joint and followed to its insertion on the third metacarpal bone. Lateral to the radial carpal extensor tendon, the common digital extensor tendon was detected and both tendons could be discriminated on the T1-, T2-, and PD-weighted images due to their clear borders and uniform hypointensity in relation to the surrounding structures (Fig. 4).

The oblique carpal extensor tendon was hypointense and was infrequently seen on either the latero-distal aspect of radius or medial to the metacarpus. Both the lateral digital extensor and the ulnar carpal extensor tendons expressed homogenous hypointensity on either of the T1- weighted, T2- weighted, or PD- weighted MRI images. The ulnar carpal flexor tendon was traced palmaro-laterally and the radial carpal flexor tendon was assessed palmaro-medially with uniform clear borders and showed hypointense signals on the T1-, T2-, and

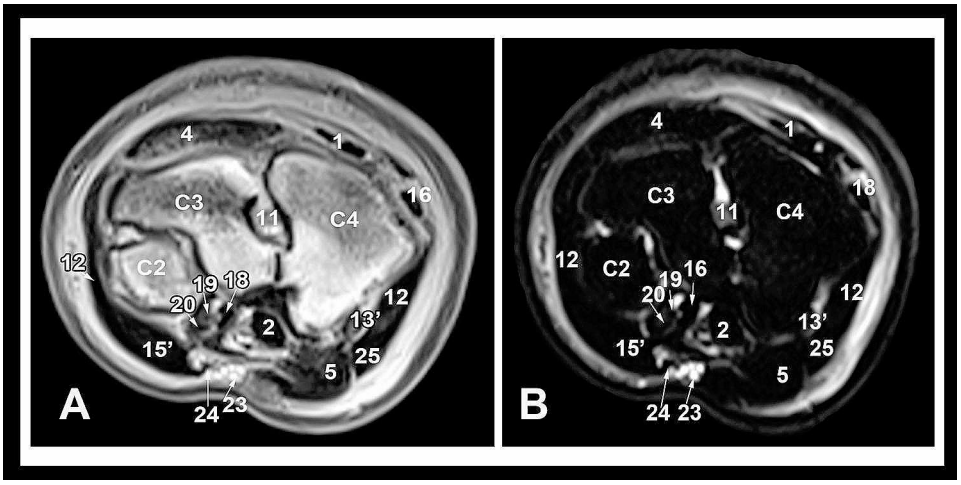

Fig. 6 Transverse T1-weighted (**A**) and STIR (**B**) high-filed MRI images at the level of the distal row of carpal bones. Medial is to the left. C2, 2nd carpal bone; C3, 3rd carpal bone; C4, 4th carpal bone; 1, common digital extensor tendon; 2, deep digital flexor tendon; 4, radial carpal extensor tendon; 5, superficial digital flexor tendon; 11, short inter-carpal ligament; 12, long lateral collateral carpal ligament; 13′, short lateral collateral carpal ligament; 14, long medial collateral carpal ligament; 15′, short medial collateral carpal ligament;16, lateral digital extensor tendon; 18, radial carpal flexor tendon; 19, median artery; 20, median vein; 23, radial artery; 24, radial vein; 25, accessoriometacarpal ligament

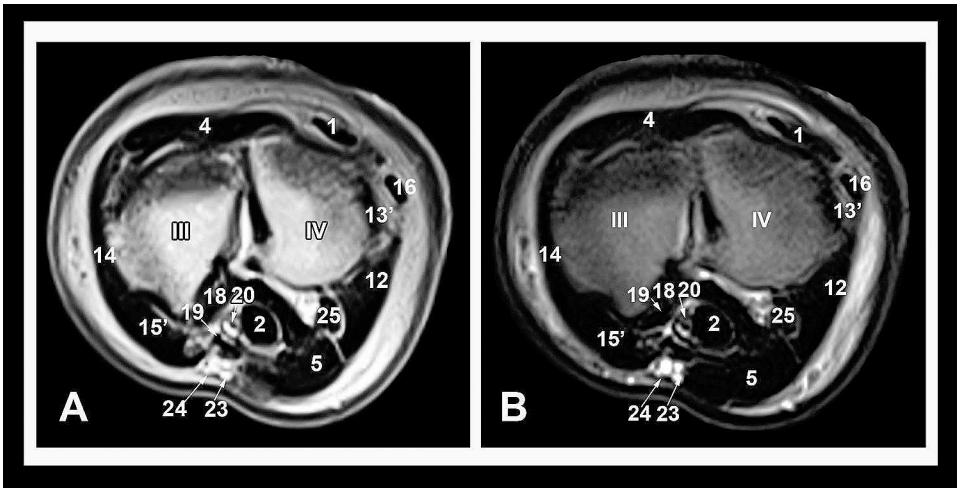

Fig. 7 Transverse T1 (**A**) and PD-weighted (**B**) high-filed MRI images at the level of the proximal metacarpal region. Medial is to the left. III, 3rd metacarpal bone; VI, 4th metacarpal bone; 1, common digital extensor tendon; 2, deep digital flexor tendon; 4, radial carpal extensor tendon; 5, superficial digital flexor tendon; 12, long lateral collateral carpal ligament; 13′, distal part of the short lateral collateral carpal ligament; 14, long medial collateral carpal ligament; 15′, distal part of the short medial collateral carpal ligament; 16, lateral digital extensor tendon; 18, radial carpal flexor tendon; 19, median artery; 20, median vein; 23, radial artery; 24, radial vein; 25, accessoriometacarpal ligament

PD- weighted MRI images. The SDFT and DDFT were depicted palmary on the carpus and showed homogeneous hypointensity. The flexor retinaculum enclosed the palmar structures of the carpus and presented homogeneous hyperintensity on all pulse sequences (Figs. 5 and 6).

The dromedary camel collateral carpal ligaments comprised of the medial and lateral collateral parts on either side of the joint. Each collateral ligament presented a superficial long division and deep short subdivisions that could be seen and discriminated on the MRI images. On the medial side of the joint, the long collateral division originated from the medial radial styloid process and terminated disto-palmarly on the medio-palmar crest of the metacarpus, where it was blended to the origin of the SDFT (Fig. 7). The short fascicles of the medial collateral ligament were connected to the radial, the second and third carpal bones. The medial and lateral collateral carpal ligaments exhibited heterogeneous signal intensity at its origin and insertion and homogenous hypointensity during its course on the medial and lateral aspects of the carpus, on all MRI sequences. On the medio-palmar crest of the metacarpus, the insertion of the medial collateral ligament and the origin of the SDFT could not be

differentiated. The lateral collateral ligament commenced at the lateral styloid process and terminated on the proximal end of the lateral metacarpal bone. The deep short bands of the lateral collateral division stretched between the radius and the ulnar carpal bone; connected among the ulnar and the fourth carpal bones; and attached between the fourth carpal bone and the proximal metacarpus.

Ligaments supporting the accessory carpal bone (the accessory ulnar, the accessory carpoulnar, the accessory quartal and the accessory metacarpal ligaments) exhibited heterogeneous signal intensity and could be seen in the sagittal and transverse MRI images. The palmar carpal ligaments and the transverse inter-carpal ligaments expressed intermediate intensity on the T1 and T2 images and were best assessed on the dorsal and transverse plane images. Dorsally on the carpus, a fat pad of variable size and heterogeneous intensity was depicted in the dorsal aspect of the carpus at the level of the antebrachiocarpal and midcarpal joints.

The antebrachiocarpal joint had a small dorsal pouch and a large palmar pouch, contains some synovial fluid. The midcarpal joint also had a small dorsal pouch with a minimal amount of synovial fluid, and a larger palmar pouch. The lateral palmar pouch was markedly extended and could be recognized below the accessory carpal bone between the lateral collateral ligament and the ulnar carpal extensor. The dorsal pouch of the carpometacarpal joint contains minimal synovial fluid. Its palmar pouch extends distally to a variable degree on both medial and lateral sides. Synovial fluid had high signal intensity on PD, T2, and STIR images and intermediate signal intensity on T1 images. The pre-carpal bursa was difficult to identify in normal camels, although on T2 and PD images it might be possible to visualize small amounts of fluid near the proximal and distal extents.

Discussion

To the best of our knowledge, the present study is the first report describing the MRI features of the dromedary camel carpal articulations. The developed MRI protocol in this study was valuable for defining the signal intensity of the most significant structures in the carpal region. It permitted a distinctive depiction of articular cartilage, cortical and subchondral bone as well as the ligamentous and tendinous structures, which is not completely possible by other diagnostic modalities. The obtained results are in agreement with previous reports in horses and cattle confirming that MRI offers the best evaluation technique for all anatomical structures in the carpal joint, particularly the soft tissue structures [5, 8, 15]. The MRI sequences used in this study were selected as they were successfully used for assessment of the carpal region in equine, bovine and canine [15–17]. The MRI settings were reflective of the parameters used in equine orthopedic MRI and the acquisition durations for the used sequences were satisfactory if used in clinical patients [18]. The resultant images afforded excellent definition and the bony and soft tissue structures were definitely recognizable. Although T1, T2, PD and STIR imaging sequences were produced for this study, the T1 and PD images showed superior anatomic description. T2 weighted images were of great value concerning synovial structures and STIR images were informative for the high fat content structures [8].

In this study, all bones of the camel carpus were easily recognized and the signal intensity of each individual structure could be determined. The radial and metacarpal medulla expressed hyperintensity, the carpal articular cartilage showed intermediate signal intensity and the cortical bone exhibited hypointensity on T1 and T2 sequences. These findings shared similarity with horses [5] and cattle [15]; however, in horses, the distal row of carpal bones includes an additional bone, the first carpal bone [19] and the carpometacarpal articular cartilage was not seen clearly [5]. In cattle, the second and third carpal bones are united [20].

Carpal tendons in the current study had clear margins, homogenous hypointensity and could be discriminated and traced on each side of the carpal region. Dorsally on the carpus, the radial carpal extensor, common digital extensor and the lateral digital extensor tendons could be evaluated. Caudo-laterally, the ulnar carpal extensor and ulnar carpal flexor tendons were outlined. While palmary, the radial carpal flexor, SDFT and DDFT tendons were investigated. In horses and cattle [5, 15], the flexor and extensor tendons showed similar attitude; however, the SDFT in these species contained considerable amount of muscular tissue that appeared as areas of intermediate signal intensity in T1 and T2 sequences. In dromedaries, the proximal muscular part of the superficial digital flexor muscle is absent and the SDFT arises from the accessory carpal bone [1].

In horses, MRI is the cornerstone for investigation of soft tissue disorders [21]. MRI showed numerous merits compared with the other traditional (radiography/ultrasonography) or recent (nuclear scintigraphy/computed tomography) diagnostic imaging modalities. MRI is non-invasive, biologically safe and affords multi-planar three-dimensional imaging capabilities. MRI enables visualization of both bones and soft tissues concurrently and discriminates the diseased area out of the surrounding normal tissues by using of various imaging sequences. Although computed tomography can be used to evaluate bone and soft tissues, MRI provides superior soft tissue contrast than computed tomography [22]. Currently, development of practical MRI in dromedary camels remained in its infancy and optimization of the use of

MRI techniques is still in progress: however, its use for evaluation of certain regions in camels was performed successfully [23]. We believe that this technique could revolutionize the assessment of certain musculoskeletal lesions in camels, particularly athletic camels.

Carpal lameness may occur in camels of all breeds and disciplines but it is most prevalent in athletic camels. Repetitive impact loading on the carpus during training and racing may lead to subchondral bone sclerosis and may result in osteochondral fragmentation, osteoarthritis and carpal bone fractures. Carpal lameness may also result from trauma due to falls or other injuries. While many of these injuries can be evaluated sufficiently well using radiography and ultrasonography, MRI seems to be useful to further evaluate the extent of injury. Furthermore, MRI may demonstrate pathology in the absence of positive findings with other imaging tools.

Conclusions

This study portrayed camel carpal joint in multiple sequences and planes and revealed variability in the MRI appearance of the soft-tissue and bone structures of the dromedary camel carpal joint. T1- weighted and PD sequences were useful for bone and soft tissue evaluation and produced high-resolution anatomic images with relatively good signal strength. T2-weighted images were particularly useful for evaluating synovial structures. Precise analysis of clinical MRI examinations necessitates a deep knowledge of the normal MRI features of various structures in the region of interest. The obtained images are thought to be of value for understanding other diagnostic imaging modalities and could be supportive for interpretation in clinical circumstances.

Methods

Animals

Twelve forelimbs (6 left and 6 rights) were harvested from 6 clinically normal adult camels (3 males and 3 non pregnant females; age range, 8–14 years; and weight, 430–570 kg). Camels were belonging to the farm of the King Faisal University and were euthanized at the Veterinary Teaching Hospital, College of Veterinary Medicine, King Faisal University for reasons unrelated to the study or orthopedic problems. Animals were euthanized by IV injection of sodium pentobarbital in a dose rate of 40 mg/kg. Instantly after euthanasia, limbs were disarticulated at the shoulder joint and scanned fresh within 2 h to avoid imaging artifacts. Limbs were physically examined and radiographed and no abnormalities were identified.

MRI protocol

The limbs were placed on the lateral side in the central bore of a 1.5 Tesla Magnetom Sempra MRI system (Siemens Healthcare GmbH, Erlangen, Germany) using human extremity coil. An initial three-plane localizer image was acquired to confirm accurate limb placing and sequence alignment. The scanning sequence protocol was T1-weighted (T1), T2-weighted (T2), proton density-weighted (PD) turbo spin echo (TSE) and Short Tau Inversion Recovery (STIR). In each MRI sequence, the carpal region was scanned in transverse, sagittal and dorsal planes from the distal aspect of the radius to the proximal metacarpal region. The sagittal slices were aligned perpendicular to the palmar aspect of the carpal bones along the long axis of the limb, and the transverse slices were aligned perpendicular to the dorsal aspect of the carpus on the sagittal image and parallel to the carpal joint spaces on the dorsal image. The dorsal slices were obtained from the dorsal aspect of the carpus to the palmar aspect of the carpal bones and were aligned parallel to the dorsal aspect of the carpus (Fig. 1). The technical parameters for each MRI sequence are summarized in Table 1.

Survey computed tomography

Three cadaveric limbs were scanned using a multi-detector CT scanner (Siemens; Siemens GmbH, Germany). The scanner settings were: 100 kV, 100 mA, slice thickness of 3 mm, window width of 2700 and window level of 350 Hounsfield Units and matrix size of 512 pixels. Images were reconstructed and a three-dimensional image was generated to demonstrate the levels of the selected MRI images.

MRI interpretation

The obtained MRI images were analyzed, various soft and osseous structures were recognized and the signal intensity of individual structure on each MRI sequence was evaluated and recorded. MRI imaging findings were reviewed by the authors. If a discrepancy in opinion was evident, authors met and a consensus opinion was formulated.

Table 1 High-field 1.5 Tesla MRI parameters for examination of the dromedary camel carpal joint

Sequence	Echo time (msec)	Repetition time (msec)	Flip angle	Field of view	Matrix Size	Slice thickness (mm)	Gap (mm)
T1	28	670	90°	512×512	192×136	4	1
T2	120	4175	90°	24×18.4	256×256	4	1
PD	100	2370	90°	24×24	192×256	4	1
STIR	45	1490	90°	24×24	192×256	4	1

Abbreviations

MRI	Magnetic resonance imaging
CT	Computed tomography
TSE	Turbo Spin-echo
T1	T1- weighted turbo spin echo
T2	T2- weighted turbo spin echo
PD	PD- - weighted turbo spin echo
STIR	Short Tau inversion recovery
SI	Signal intensity
DDFT	Deep digital flexor tendon
SDFT	Superficial digital flexor tendon

Acknowledgements
The author thanks the Deanship of Scientific Research, Vice Presidency for Graduate Studies and Scientific Research, King Faisal University, Saudi Arabia for the financial support.

Author contributions
A.E. and U.H. designed the study, optimized and acquired MR settings, data analysis and interpretation, and drafted the manuscript. U.H reviewed, edited and submitted the manuscript. All authors reviewed the final version of the manuscript.

Funding
This work was supported by the Deanship of Scientific Research, Vice Presidency for Graduate Studies and Scientific Research, King Faisal University, Saudi Arabia (Grant KFU241282).

Data availability
The datasets used and/or analyzed during the current study are available from the corresponding author on reasonable request.

Declarations

Ethics approval and consent to participate
The present study was permitted by the Research Ethics Committee (REC) of King Faisal University, KSA (Permit Number: KFU-REC/2022-01-08). All procedures were carried out in accordance with the relevant guidelines and regulations. All methods are reported in accordance with ARRIVE guidelines for the reporting of animal experiments.

Consent for publication
Not applicable.

Competing interests
The authors declare no competing interests.

Received: 20 April 2023 / Accepted: 8 July 2024
Published online: 06 September 2024

References

1. Smuts MS, Bezuidenhout AJ. Anatomy of the Dromedary. Oxford: Clarendon; 1987. pp. 54–104.
2. Kassab A. The normal anatomical, radiographical and ultrasonographic appearance of the carpal region of one-humped camel (camelus dromedarius). Anat Histol Embryol. 2008;37:24–9.
3. Badawy AM, Marzok MA, Eshra EA. Computed tomographic arthrography of the normal dromedary camel carpus. Vet Comp Orthop Traumatol. 2016;29:188–94.
4. Kofler J. Ultrasonographic Examination of the Carpal region in cattle—normal appearance. Vet J. 2000;1:85–96.
5. Nagy A, Dyson S. Magnetic resonance anatomy of the carpus of the horse described from images acquired from low-field and high-field magnets. Vet Radiol Ultrasound. 2011;52:273–83.
6. Mair TS, Kinns J, Jones RD, Bolas NM. Magnetic resonance imaging of the distal limb of the standing horse. Equine Vet Edu. 2005;17:74–8.
7. Brokken MT, Schneider RK, Sampson SN, Tucker RL, Gavin PR. Magnetic resonance imaging features of proximal metacarpal and metatarsal injuries in the horse. Vet Radiol Ultrasound. 2007;48:507–17.
8. Sanchez-Andrade JS, Richter H, Kuhn K, Bischofberger AS, Kircher PR, Hoey S. Comparison between magnetic resonance imaging, computed tomography, and arthrography to identify artificially induced cartilage defects of the equine carpal joints. Vet Radiol Ultrasound. 2018;59:312–25.
9. Getman LM, Mcknight AL, Richardson DW. Comparison of magnetic resonance contrast arthrography and arthroscopic anatomy of the equine palmar lateral outpouching of the middle carpal joint. Vet Radiol Ultrasound. 2007;48:493–500.
10. Gonzalez LM, Schramme MC, Robertson ID, Thrall DE, Redding RW. MRI features of metacarpo(tarso)phalangeal region lameness in 40 horses. Vet Radiol Ultrasound. 2010;51:404–14.
11. Powell SE, Ramzan PL, Head MJ, Shepherd MC, Baldwin GI, Steven WN. Standing magnetic resonance imaging detection of bone marrow oedema-type signal pattern associated with subchondral bone pain in 8 racehorses: a prospective study. Equine Vet J. 2010;42:10–7.
12. Waselau M, McKnight A, Kasparek A. Magnetic resonance imaging of equine stifles: technique and observations in 76 clinical cases. Equine Vet J. 2020;32:85–91.
13. Tucker RL, Sampson SN. Magnetic resonance imaging protocols for the horse. Clin Tech Equine Pract. 2007;6:2–15.
14. Ibrahium AM, Shaker NA. Gross anatomical structure and magnetic resonance images of the carpal joint in one humped camel (Camelus dromedarius) and its arterial blood supply. Inter J Vet Sci. 2018;7:12–7.
15. Hagag U, El Nahas A, Almohamad ZA, Brehm W, Gerlach K. 3T magnetic resonance imaging and computed tomography of the bovine carpus. BMC Vet Res. 2022;18:236–45.
16. Anastasiou A, Skioldebrand E, Ekman S, Hall LD. Ex vivo magnetic resonance imaging of the distal row of equine carpal bones: Assessment of bone sclerosis and cartilage damage. Vet Radiol Ultrasound. 2003;44:501–12.
17. Castelli E, Pozzi A, Klisch K, Scotti L, Hoey S, Dennler M. Comparison between high-field 3 Tesla MRI and computed tomography with and without arthrography for visualization of canine carpal ligaments: a cadaveric study. Vet Surg. 2019;48:546–55.
18. Murray R, Dyson S, Branch M, Schramme M. Validation of magnetic resonance imaging use in equine limbs. Clin Tech Equine Pract. 2007;6:26–36.
19. Budras K, Sack W, Rock S. Anatomy of the horse. 5th ed. Hannover: Schlütersche Verlagsgesellschaft GmbH & Co. KG; 2011. pp. 16–31.
20. Dyce KM, Sack WO, Wensing CJG. Textbook of Veterinary anatomy. Missouri: Saunders, Elsevier; 2010. pp. 215–380.
21. Bubeck KA, Aarsvold S. Diagnosis of soft tissue injury in the sport horse. Vet Clin North Am Equine Pract. 2018;34:215–34.
22. Nelson BB, Kawcak CE, Barrett MF, McIlwraith CW, Grinstaff MW, Goodrich LR. Recent advances in articular cartilage evaluation using computed tomography and magnetic resonance imaging. Equine Vet J. 2018;50:564–79.
23. Al Mohamad ZA, Hagag U, El Nahas A. Magnetic resonance imaging of the normal dromedary camel tarsus. BMC Vet Res. 2021;17:101.

Publisher's Note